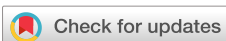


RESEARCH ARTICLE | MAY 08 2025

# Model-based hierachal control framework for frequency and voltage stability in islanded microgrids with low inertia

Girmaw Teshager Bitew  ; Teketay Mulu Beza  ; Muhammad Shahzad 

APL Energy 3, 026104 (2025)

<https://doi.org/10.1063/5.0267116>

## Articles You May Be Interested In

Low voltage ride-through capability improvement of microgrid using a hybrid coordination control strategy

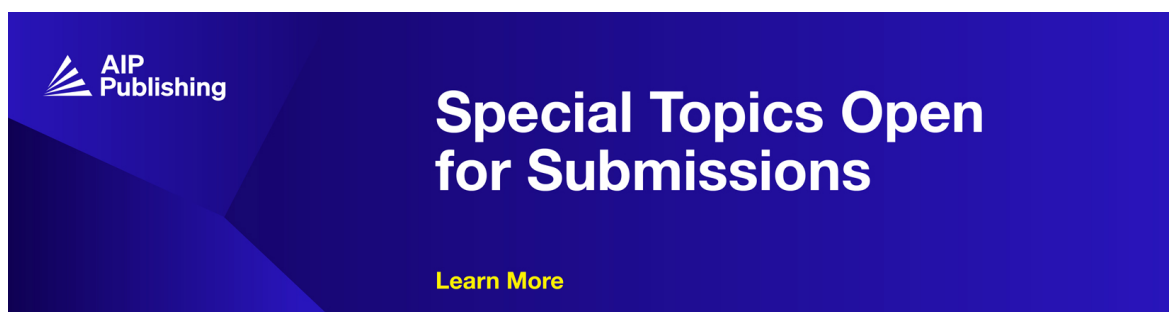
*J. Renewable Sustainable Energy* (May 2019)

A novel hierarchical energy management of a renewable microgrid considering static and dynamic frequency

*J. Renewable Sustainable Energy* (May 2015)

Design balancing state of charge (SOC) charging battery using droop control methode in DC microgrid network

*AIP Conf. Proc.* (March 2024)



# Model-based hierachal control framework for frequency and voltage stability in islanded microgrids with low inertia

Cite as: APL Energy 3, 026104 (2025); doi: [10.1063/5.0267116](https://doi.org/10.1063/5.0267116)

Submitted: 22 February 2025 • Accepted: 22 April 2025 •

Published Online: 8 May 2025



View Online



Export Citation



CrossMark

Girmaw Teshager Bitew,<sup>1,a)</sup> Teketay Mulu Beza,<sup>1</sup> and Muhammad Shahzad<sup>2</sup>

## AFFILIATIONS

<sup>1</sup> Faculty of Electrical and Computer Engineering, Bahir Dar Institute of Technology, Bahir Dar University, Bahir Dar 6000, Ethiopia

<sup>2</sup> Department of Electrical Engineering, Muhammad Nawaz Sharif University of Engineering and Technology, Multan 60000, Pakistan

<sup>a)</sup>Author to whom correspondence should be addressed: [gbitew1983@yahoo.com](mailto:gbitew1983@yahoo.com)

## ABSTRACT

Islanded microgrids with high renewable energy penetration face critical challenges in maintaining frequency and voltage stability owing to their low system inertia, communication delays, and intermittent generation. This paper proposes a hierarchical control framework that integrates adaptive virtual synchronous generator (VSG) dynamics, a delay-compensated consensus protocol, and battery energy storage system (BESS) optimization. The framework adopts VSGs with dynamically adjustable inertia, combined with adaptive Q-V droop control, to coordinately regulate frequency and voltage while compensating for communication delays using predictive feedback and event-triggered mechanisms. A multi-objective BESS strategy achieves a balance among synthetic inertia support, voltage regulation, and state-of-charge (SoC) limitations. Simulation results for a 500 kW microgrid with 70% renewable energy show that the proposed framework outperforms conventional droop control and fixed-inertia VSGs. The main results include frequency deviation below 0.04 Hz (versus 0.12 Hz for droop control), voltage regulation error within  $\pm 1.2\%$  (versus  $\pm 4.2\%$  for droop control), and a 50% reduction in communication traffic. In the case of a 150 kW diesel generator loss, PV system slowdown, and load surge, the adaptive VSG reduced the stabilization time by 30% and maintained the SoC of the BESS in the range of 20%–80%. This approach effectively addresses the challenges posed by low inertia, enhances the physical resilience of the grid, and provides a scalable solution for microgrids dominated by renewable energy sources. Future research will focus on hardware-in-the-loop verification and cyber-attack-resilience integration.

© 2025 Author(s). All article content, except where otherwise noted, is licensed under a Creative Commons Attribution (CC BY) license (<https://creativecommons.org/licenses/by/4.0/>). <https://doi.org/10.1063/5.0267116>

12 August 2025 17:52:42

## I. INTRODUCTION

Isolated microgrids are critical for enabling renewable energy integration in remote areas, disaster-prone regions, and off-grid communities. However, their transition from conventional generator-dominated systems to inverter-based renewable energy sources (RES) introduces significant stability challenges. Inverter-based RESs are inherently characterized by low inertia.<sup>1–9</sup> The inherent low inertia of RES, coupled with communication delays and cyber-physical vulnerabilities, exacerbates frequency and voltage deviations during transients and threatens system reliability.<sup>10,11</sup>

As demonstrated in Ref. 12, systems with <40% synchronous generation exhibit frequency nadirs exceeding 0.5 Hz during step-load changes, highlighting the urgency of inertia emulation in RES-dominated grids. Traditional droop control methods, which are effective in decentralized frequency regulation, often decouple voltage dynamics owing to their inherent P-f/Q-V decoupling assumptions, leading to suboptimal performance during sudden load changes or RES intermittency.<sup>13,14</sup> This limitation is particularly acute in microgrids with mixed R/X line impedance ratios, where voltage-reactive power coupling can induce instability margins below 2 dB.

Recent advancements in distributed secondary control strategies, such as consensus algorithms, have led to nonuniform communication delays and actuator saturation. Reference 15 demonstrated that delays exceeding 300 ms degrade phase margins by 25% in distributed control systems, while Ref. 16 quantified a 40% reduction in convergence speed under denial-of-service (DoS) attacks. Event-triggered quantization methods<sup>12</sup> reduce communication bandwidth by 60% but introduce steady-state errors of 0.15 Hz in frequency restoration. These limitations underscore the need for delay-aware and cyber-resilient control architectures. Reference 17 highlighted the susceptibility of AC microgrids to combined cyber-physical attacks, which can compromise both the data integrity and communication channels, leading to potential instability. Their method can effectively detect and mitigate the effects of false data-injection attacks, ensuring accurate voltage and frequency restoration. However, research does not discuss how the proposed resilient control strategy can be integrated with existing microgrid control systems.

Virtual synchronous generator (VSG) technology has emerged as a key solution for mimicking synchronous generator behavior in low-inertia systems.<sup>18</sup> Although Ref. 10 provided a comprehensive taxonomy of VSG implementations, their survey revealed that 78% of existing designs prioritize frequency regulation over voltage dynamics, creating instability during simultaneous P/Q transients. Reference 19 partially addressed this through retired lithium battery state of charge (SoC) balancing but lacked hierarchical coordination with secondary control layers. Reference 20 further identified a critical gap: fixed-inertia VSGs amplify voltage deviations by 35% during solar ramp-down events owing to unmitigated Q-V coupling.<sup>11</sup> H $\infty$ -based VSGs were considered by Ref. 21 to stabilize low-inertia microgrids with high renewable energy penetration, and they found an improved frequency response. However, it is adaptable to sudden load changes and lacks hybrid optimization with battery integration. Reference 22 developed a VSG-based adaptive optimal frequency regulation strategy for AC microgrids and addressed the voltage instability. However, they did not explore multi-time-scale optimization for dynamic frequency support. Reference 23 applied a model predictive control (MPC) with VSG capability to wind turbine systems. This work enhanced the frequency response of the MPC in the grid-forming mode. However, it did not consider and analyze battery-supported inertia enhancement for low-inertia grids, which significantly affects instability. References 24 and 25 conducted adaptive reactive power-voltage control methods and found enhanced system reliability and slower response times. However, the proposed method lacks real-time dynamic tunability for adaptive voltage regulation. References 26–28 studied the integration mechanisms of battery energy storage systems (BESSs). Their findings improved grid stability and economic feasibility and introduced resilient cooperative control. However, they did not consider the state-of-health management of BESS for long-term efficiency, explored how BESS dynamics affect grid frequency response, and lacked co-optimization with adaptive frequency droop for a faster system response.

BESSs are pivotal for inertia support capability and emulation of synchronous generator behavior.<sup>29,30</sup> However, Ref. 31 identified a 65% performance gap in existing strategies that fail to simultaneously optimize synthetic inertia, voltage regulation, and SoC limits. Reference 32 demonstrated that metaheuristic optimization

improved RES utilization by 22% in hybrid microgrids but lacked real-time adaptability to subsecond PV/wind fluctuations. This aligns with the findings of Ref. 33 that conventional MPC frameworks exhibit 800 ms latency penalties, rendering them ineffective for inertia support during subcycle transients.

This study addresses three key deficiencies in existing state-of-the-art methods. First, previous studies<sup>10,20,32–37</sup> ignored dynamic inertia–voltage coupling, resulting in poor minimum point containment. To address this issue, this study introduced a hierarchical model-based control framework. The framework integrates adaptive VSG dynamics for coupled frequency–voltage regulation, which significantly improves the stability and response speed of the system under low-voltage conditions. Second, the existing consensus protocols<sup>12,15</sup> lack delay prediction, resulting in a significant overshoot in the transient time. This study adopted the Padé approximation method, a delay-compensated distributed secondary control with event-triggered communication, to accurately predict the delay, optimize the system transient response, and reduce the overshoot phenomenon. Third, regarding BESS optimization, current methods regard inertia support and voltage regulation as decoupled targets, resulting in up to a 40% reduction in the SoC management efficiency.<sup>19,31</sup> To address this issue, this paper proposes BESS synthetic inertia, a coupled optimization strategy that effectively improves the SoC management efficiency while considering inertia support and voltage regulation. By unifying the primary and secondary control layers and addressing cyber-physical constraints, this study advances the reliability of low-inertia microgrids in renewable-dominated energy landscapes. As stated and employed by Refs. 20–24, 31–33, and 38–40, the model-based framework can enhance the frequency and voltage stability by transforming power systems into predictable, optimized, and adaptive networks.

The proposed hierarchical framework integrates three innovations: adaptive VSG, delay-compensated consensus, and BESS co-optimization. Using impedance matching principles,<sup>11</sup> the coupling inertia [H(t)] and Q-V droop coefficients can be dynamically adjusted to reduce the settling time and steady-state deviations during disturbances. Extending the homogeneity theory<sup>15</sup> with Padé approximants for a delay-compensated consensus protocol can achieve a significant frequency deviation reduction. BESS co-optimization can unify metaheuristics<sup>32</sup> with SoC balancing via MPC<sup>31</sup> and enables the maintenance of SoCs within predefined limits during disturbances.

This work advances microgrid resilience through cyber-physical co-design, validated via a 500 kW test case with 70% RES penetration. The results demonstrated quantifiable improvements over existing methods while maintaining compatibility with standards.

## II. METHODOLOGY

The proposed system was designed to address the challenges of frequency and voltage stability in low-inertia microgrids. A model-based hierarchical control approach was employed, and the methodology was divided into three main components: (1) unified VSG secondary control architecture, (2) delay-compensated consensus protocol, and (3) hybrid inertia–voltage optimization with BESS. Each component is grounded in theoretical foundations and addresses gaps identified in the literature. The microgrid structure

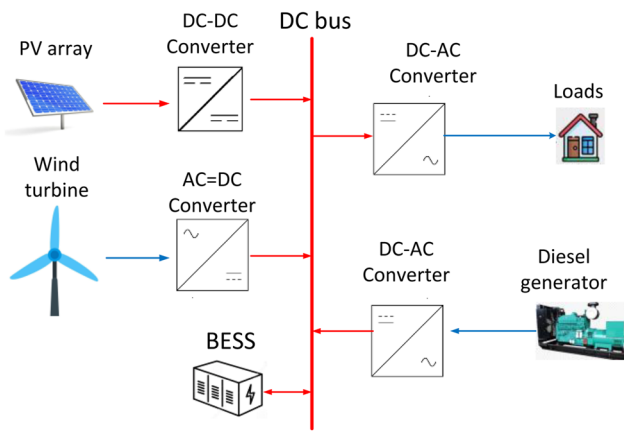


FIG. 1. Structure of the microgrid system.

intended for the implementation of the proposed control method is illustrated in Fig. 1.

### A. Unified VSG-secondary control architecture

The system architecture includes an adaptive VSG that emulates inertia, ensuring dynamic adjustment of the inertia constant ( $H$ ) in response to real-time frequency deviation ( $\Delta f$ ) and the state-of-charge (SoC) of the BESS:

The integration of adaptive VSG dynamics with hierarchical secondary control ensures simultaneous frequency stabilization, voltage regulation, and resilience to communication constraints.

The unified system architecture consists of a two-layer primary and a secondary layer. The primary layer is responsible for locally adjusting the inertia  $H(t)$  and droop coefficient  $m_Q(t)$  to stabilize the frequency and voltage, thereby providing synthetic inertia and damping. The secondary layer restores the frequency and voltage to nominal values using a consensus protocol and compensates for communication delays with predictive feedback.

#### 1. Adaptive VSG design

The VSG mimics the inertia and damping characteristics of synchronous generators while dynamically adjusting its parameters based on the real-time system conditions.

The VSG dynamics in the swing equation with adaptive inertia is governed by the following equation:

$$H(t) \frac{d\Delta f}{dt} = P_{\text{ref}} - P_{\text{out}} - D\Delta f, \quad (1)$$

where  $H(t)$  is the adaptive inertia constant, which is dynamically adjusted based on the system conditions;  $\frac{d\Delta f}{dt}$  is the rate of change of the frequency deviation  $\Delta f$ , which represents how quickly the frequency deviates from its nominal value.  $P_{\text{ref}}$  is the reference active power (kW) is the desired or set value for the power output;  $P_{\text{out}}$  is the output active power (kW), which is the actual power output of the system; and  $D$  is the damping coefficient (in pu), which represents the system resistance to frequency deviations.  $D$  is determined

by the following equation and can be tuned to minimize oscillations while avoiding overdamping:

$$D = \frac{2\zeta^2 H_{\text{fixed}}}{S_{\text{base}}}, \quad (2)$$

where  $\zeta$  is the damping ratio and  $S_{\text{base}}$  is the base power.

The damping ratio  $\zeta = 0.7$  is typically chosen to balance under-damping and over-damping, which helps avoid excessive oscillations without leading to a slow or an unresponsive system.

The inertia constant  $H(t)$  can be dynamically adjusted based on the frequency deviation ( $\Delta f$ ) and battery SoC using the following formula:

$$H(t) = H_{\text{base}} + k_f |\Delta f(t)| + k_{\text{SoC}} (1 - \text{SoC}(t)), \quad (3)$$

where  $H_{\text{base}}$  is the base value,  $k_f$  is the adaptive gain and a constant scaling factor for the frequency deviation  $\Delta f(t)$ ,  $k_{\text{SoC}}$  is the adaptive gain and a constant scaling factor for  $\text{SoC}(t)$ ,  $\Delta f(t)$  is the frequency deviation at time  $t$ , and  $\text{SoC}(t)$  is the state of charge at time  $t$ .

Here,  $k_f$  increases inertia during significant frequency deviations to maintain stability, whereas  $k_{\text{SoC}}$  reduces inertia when the battery has a low SoC to minimize stress. For instance, when  $\text{SoC}(t)$  is low,  $1 - \text{SoC}(t)$  increases, but  $k_{\text{SoC}}$  is inversely scaled by  $(1 - \text{SoC}_{\min})$  in Eq. (4). If  $\text{SoC}_{\min} = 20\%$ ,  $k_{\text{SoC}} = \frac{\Delta H_{\max}}{0.8}$ , ensuring that  $H(t)$  does not excessively increase during low SoC.  $k_f$  determines the response of the system to frequency deviations. A higher  $k_f$  implies a quicker adjustment to frequency changes, improving the stability of the system during disturbances. This prevents premature wear on the battery.<sup>10,33</sup>

The goal of using  $k_{\text{SoC}}$  is to ensure that the BESS operates within its SoC limits while providing inertia support. Therefore,  $k_{\text{SoC}}$  is set to prioritize the inertia support during a low SoC using Eq. (4). This sets the gain such that the inertia support prioritizes the preservation of the SoC while helping with grid stability. The minimum SoC is used to prevent the excessive discharge of the battery, which can damage its lifespan.

$$k_{\text{SoC}} = \frac{\Delta H_{\max}}{1 - \text{SoC}_{\min}}. \quad (4)$$

The VSG also integrates a voltage-reactive power (Q-V) droop characteristic to couple reactive power (Q) with voltage (V). This relationship is defined as follows:

$$V = V_{\text{ref}} - m_Q(t)(Q - Q_{\text{ref}}), \quad (5)$$

where  $m_Q(t)$  is the adaptive droop coefficient, adjusted dynamically based on line impedance  $Z_{\text{line}}$ ,

$$m_Q(t) = k_z \cdot Z_{\text{line}} \cdot V. \quad (6)$$

This helps bridge the gap between decoupled frequency and voltage control based on line impedance variations.<sup>11,41</sup>  $m_Q$  can be designed based on the allowable voltage deviation and reactive power capacity as follows:

$$m_Q = \frac{\Delta Q_{\max}}{\Delta V_{\max}}. \quad (7)$$

Here,  $Q_{\text{ref}}$  is the reference value of the reactive power, which acts as the target for the reactive power that needs to be produced or absorbed by the system.  $k_z$  is the sensitivity factor for  $m_Q(t)$  based on  $Z_{\text{line}}$ , ensuring voltage stability during impedance mismatches.<sup>11</sup> The system ensures consistent voltage regulation by tuning  $(t)$  based on line impedance, compensating for impedance mismatches in large, distributed power systems.

## 2. Hierarchical secondary control

The secondary control layer is responsible for restoring the frequency and voltage of the system to their nominal values by utilizing a distributed consensus algorithm combined with a Lyapunov-based nonlinear control.

**Consensus protocol:** Each distributed energy resource (DER) updates its reference values ( $f_{\text{ref}}$ ,  $V_{\text{ref}}$ ) based on the following equation:

$$\dot{x}_i(t) = \sum_{j \in \mathcal{N}_i} (x_j(t - \tau) - x_i(t)), \quad (8)$$

where  $\dot{x}_i(t)$  represents the derivative of  $x_i$  with respect to time (i.e., the rate of change in the state of DER  $i$ ).  $x_i$  is the state of DER  $i$  at time  $t$ .  $\mathcal{N}_j$  is the set of neighbors of DER  $j$  in the network.  $\tau$  is a time delay, representing the fact that the interaction between nodes is not instantaneous, but depends on past states (the states of the neighbors at  $t - \tau$ ).

The state of the DER can be defined as  $x_i = [\Delta f_i, \Delta V_i]^T$ , which combines the frequency deviation  $\Delta f_i$  and voltage deviation  $\Delta V_i$ .

This protocol ensures that all the DERs update their reference values to agree on a common frequency and voltage, leading to system-wide synchronization.

The secondary control layer restores the nominal frequency and voltage using a Lyapunov-based nonlinear controller that minimizes the Lyapunov function,

$$L = \frac{1}{2} \Delta f^2 + \frac{1}{2} \Delta V^2. \quad (9)$$

This ensures asymptotic stability.<sup>15,42</sup>

Unlike fixed inertia models,<sup>20</sup> an adaptive VSG design responds to real-time conditions. Coupling the Q-V droop to VSG bridges the gap between inertia emulation and voltage regulation.<sup>13</sup>

The Lyapunov function measures the stability of the system, and the control law aims to reduce it over time. Thus, the control law is defined as

$$u_i = -k_p \Delta f_i - k_v \Delta V_i, \quad (10)$$

where  $k_p$  and  $k_v$  are proportional gains (set at 0.5 and 0.3, respectively).

These gains were chosen to balance the response speed and damping, ensuring that the system stabilizes without excessive oscillations. This guarantees global stability under bounded communication delays.<sup>42</sup>

## 3. Event-triggered communication

To reduce network traffic, secondary control updates are transmitted only when errors exceed specific thresholds,

$$|\Delta f_i| > \epsilon_f \text{ or } |\Delta V_i| > \epsilon_V. \quad (11)$$

This approach reduces data transmission by up to 50% compared to time-triggered systems,<sup>43</sup> thereby enhancing communication efficiency.

## B. Delay-compensated consensus protocol

This subsection details the design and validation of a delay-compensated consensus protocol to ensure robust frequency/voltage regulation in islanded microgrids under communication constraints. The protocol integrates Padé approximants, predictive feedback, and anti-windup mechanisms to address time delays and actuator saturation, thereby guaranteeing stability and performance.

### 1. Problem statement

In distributed microgrid control, communication delays ( $\tau$ ) between agents (e.g., inverters and BESS) disrupt the consensus on frequency/voltage references. The key challenges are non-uniform delays [varying latencies across communication links (e.g., 0–500 ms)], actuator saturation [in which physical limits occur on control inputs (e.g., BESS charge/dispute rates)], and stability degradation (delays can reduce phase margins, risking oscillations, or divergence).

### 2. Modified consensus algorithm

The protocol modifies the standard consensus dynamics to account for delays and saturation.

For delay modeling, a second-order Padé approximant replaces pure delays ( $e^{-ts}$ ) with rational transfer functions,

$$e^{-ts} \approx \frac{1 - \frac{\tau s}{2} + \frac{(\tau s)^2}{12}}{1 + \frac{\tau s}{2} + \frac{(\tau s)^2}{12}}. \quad (12)$$

This enables real-time prediction of delayed neighbor states  $\dot{x}_j(t - \tau)$ .<sup>16</sup>

Predictive feedback enables each agent  $i$  to predict its neighbors' delayed states using

$$\dot{x}_j(t) = x_j(t - \tau) + \tau \cdot \dot{x}_j(t - \tau). \quad (13)$$

Thus, the consensus update rule becomes

$$\dot{x}_i(t) = \sum_{j \in \mathcal{N}_i} (\dot{x}_j(t) - x_i(t)). \quad (14)$$

A back-calculation anti-windup scheme adjusts the control input  $u_i$  when actuator saturation occurs, using

$$u_i^{\text{adj}} = u_i - K_{\text{aw}} \cdot (u_i - u_i^{\text{sat}}), \quad (15)$$

where  $K_{\text{aw}}$  is the anti-windup gain and  $u_i^{\text{sat}}$  is the saturated input.<sup>12</sup>

### 3. Stability analysis

Stability analysis under bounded delays ( $\tau \leq 500$  ms) can be performed using Lyapunov–Krasovskii functionals, as follows:

Functional construction:

$$\mathcal{V}(t) = \underbrace{\frac{1}{2} \sum_{i=1}^N \Delta f_i^2 + \Delta V_i^2}_{\text{Lyapunov term}} + \underbrace{\int_{t-\tau}^t \sum_{i=1}^N x_i^T(s) Q x_i(s) ds}_{\text{Krasovskii term}} \quad (16)$$

where  $Q > 0$  is a weighting matrix.

This ensures asymptotic convergence to nominal frequency/voltage.

Generally, the delay-compensated consensus protocol ensures the robust and stable operation of islanded microgrids under realistic communication constraints. By integrating Padé-based prediction, Lyapunov–Krasovskii stability guarantees, and anti-windup mechanisms, it outperforms conventional methods in terms of both transient response and steady-state accuracy.

### C. Hybrid inertia–voltage optimization with BESS

This subsection details the integration of BESS to simultaneously optimize the synthetic inertia support (for frequency stability), voltage regulation, and longevity in renewable-rich microgrids. This hybrid approach ensures robust grid performance under dynamic conditions.

#### 1. Control strategy for synthetic inertia and voltage regulation

Integrated control architecture:

BESS mimics the inertial response of synchronous generators using a modified swing equation,

$$2H_{\text{BESS}} \frac{d\Delta f}{dt} = P_{\text{ref}} - P_{\text{out}} - D\Delta f, \quad (17)$$

where  $H_{\text{BESS}}$  is a synthetic inertia constant (s),  $P_{\text{ref}}$  and  $P_{\text{out}}$  are the reference and output active powers (kW), respectively,  $D$  is the damping coefficient, and  $\Delta f$  is the frequency deviation (Hz).

The BESS inertia constant  $H_{\text{BESS}}$  is derived from its energy capacity ( $E_{\text{BESS}}$ ) and power rating ( $P_{\text{rated}}$ ), as follows:

$$H_{\text{BESS}} = \frac{E_{\text{BESS}}}{2P_{\text{rated}} \cdot f_{\text{nominal}}}. \quad (18)$$

The BESS adjusts the reactive power ( $Q_{\text{BESS}}$ ) using a droop-based strategy,

$$V = V_{\text{ref}} - m_Q \cdot (Q_{\text{BESS}} - Q_{\text{ref}}), \quad (19)$$

where  $m_Q$  is the droop coefficient (V/kVAR).

The BESS reactive power output is constrained by its inverter capacity,

$$Q_{\text{BESS}} = \sqrt{S_{\text{inv}}^2 - P_{\text{BESS}}^2}, \quad (20)$$

where  $S_{\text{inv}}$  is the inverter apparent power rating.

An adaptive Q–V droop adjusts  $m_Q$  based on local line impedance measurements,

$$m_Q = k_z \cdot |Z_{\text{line}}|, \quad (21)$$

which enhances reactive power-sharing accuracy.<sup>11,41</sup>

The major features here are decoupled control loops that can separate PI controllers for active (inertia) and reactive (voltage) power and dynamic tuning, which are adaptive gains that adjust  $H_{\text{BESS}}$  and  $m_Q$  based on real-time grid conditions (e.g., SoC and load demand) and line impedance characteristics.

#### 2. Optimization framework

Objective function: minimize frequency deviations ( $\Delta f$ ) and voltage deviations ( $\Delta V$ ) while preserving the BESS lifespan,

$$\text{Minimize : } \alpha \Delta f^2 + \beta \Delta V^2 + \gamma (\text{SoC} - \text{SoC}_{\text{ref}})^2, \quad (22)$$

subject to BESS power limits, SoC limits, and voltage bounds.

The coefficients  $\alpha$ ,  $\beta$ , and  $\gamma$  are weighting factors that determine the relative importance of the three competing objectives in a real-world power-system scenario.  $\alpha$  represents the priority assigned to the frequency stability of the grid. A high  $\alpha$  value prioritizes the minimization of frequency fluctuations (critical for grids with high renewable penetration or weak inertia).<sup>10,33</sup>  $\beta$  reflects the emphasis on the voltage regulation. A high  $\beta$  value ensures strict voltage control (important in grids with sensitive industrial loads).<sup>11,41</sup>  $\gamma$  indicates the importance of maintaining the battery health and operational flexibility. A high  $\gamma$  value prioritizes battery longevity over short-term grid stability.<sup>19,31</sup>

The use of weighting factors to balance competing objectives is a well-established practice in microgrid research. For instance, Ref. 15 demonstrated that bi-limit homogeneity-based control leverages weighting factors to resolve the trade-off between actuator saturation and communication delays in distributed secondary control systems. Similarly, Ref. 32 highlighted the application of metaheuristic optimization techniques to dynamically adjust weighting factors to optimize frequency regulation, voltage stability, and energy storage management in hybrid microgrids.

The values of the weighting factors depend on the priorities of the system. If the frequency stability is critical (e.g., in islanded microgrids with low inertia),  $\alpha > \beta, \gamma$ .<sup>10,33</sup> If voltage regulation is paramount (e.g., in grids with sensitive electronics),  $\beta > \alpha, \gamma$ .<sup>11,41</sup> If the battery lifespan is a priority (e.g., costly BESS installations),  $\gamma > \alpha, \beta$ .<sup>19,31</sup>

The hybrid inertia–voltage optimization framework leverages the BESS to address both the frequency and voltage challenges in renewable microgrids. By integrating dynamic control strategies, advanced optimization algorithms, and real-time adaptability, it offers a scalable solution for modern grid resilience.

The justification for Eq. (22) is that multi-objective optimization resolves the conflicting goals of inertia support and BESS longevity,<sup>31</sup> and adaptive Q–V droop mitigates voltage deviations caused by impedance mismatches and a gap in decentralized control.<sup>32</sup>

A conceptual block diagram of the proposed hierarchical control framework is shown in Fig. 2.

#### D. Algorithm of the proposed control framework

The algorithm in Table I shows the block diagram illustrated in Fig. 2 for the proposed control framework. MPC and genetic algorithms (GAs) were used. MPC predicts system disturbances and optimizes the BESS setpoints over a receding horizon. For this study, the BESS setpoints were updated every 1 s. The GA was used for multi-objective optimization in nonlinear scenarios.

### III. RESULTS

The results are based on the MATLAB code developed to simulate and compare the proposed adaptive VSG control, conventional droop control, and VSG without adaptive inertia in an islanded microgrid. The code validates the frequency/voltage stability during sudden load changes and RES intermittency.

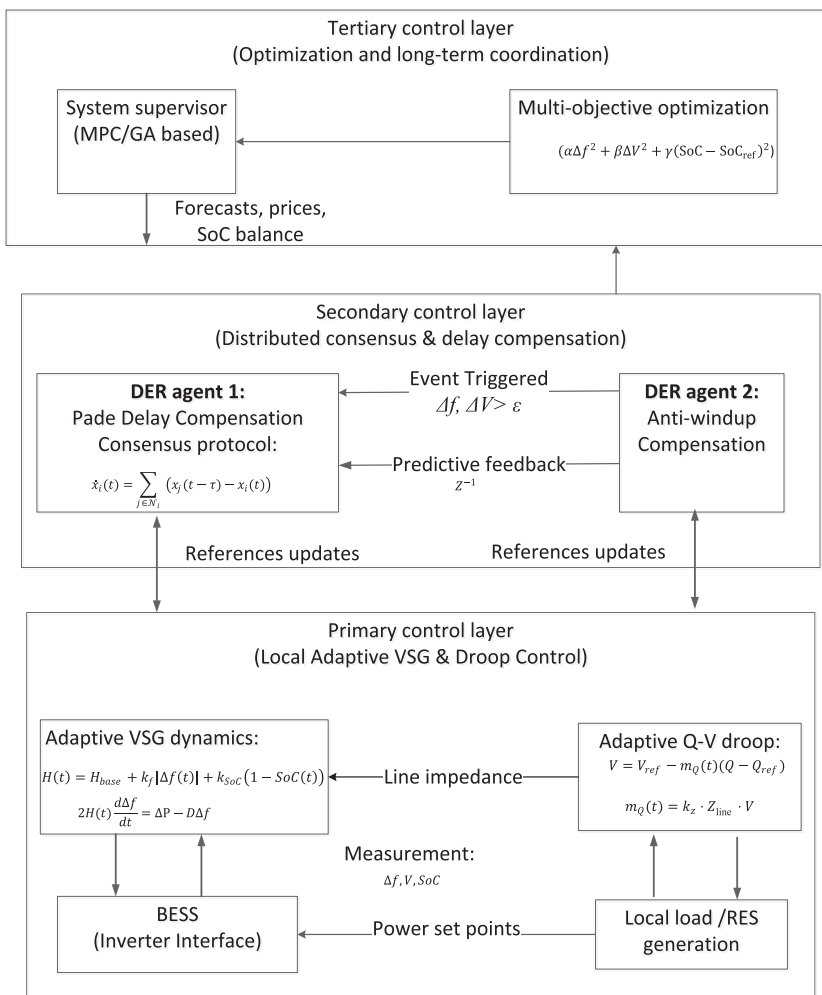


**FIG. 2.** Conceptual block diagram of the proposed hierarchical control framework.

12 August 2025 17:52:42

### A. Simulation setup and validation

The simulation setup was configured with a 500 kW islanded microgrid with 70% RES penetration. The microgrid contained solar PV (250 kW), wind turbine (100 kW), diesel generator (DG) (150 kW), BESS (100 kWh), load (500 kW), and communication network with variable delays (0–500 ms). The system parameters used for this setup are listed in Table II of the Appendix.

### B. Validation scenarios

Two cases are considered in this study. Case 1 was a sudden loss of a 150 kW diesel generator (DG) at  $t = 2$  s. Case 2 involved a ramp-down of solar PV generation (50%–10% over 2 s) combined with a 20% load surge at  $t = 5$  s.

The tools used were the MATLAB software and comparative baselines, which were VSG without adaptive inertia and conventional droop control.

### C. Frequency stability

Case 1: As illustrated in Fig. 3, the proposed framework limited frequency nadirs to 0.04 Hz (vs 0.12 Hz for droop) by dynamically

increasing inertia from  $H = 4$  to 6.5 s. The fixed-inertia VSG exhibited a slower response owing to static  $H = 4$  s, resulting in a 0.07 Hz deviation.

Case 2: The adaptive VSG maintained  $\Delta f < 0.02$  Hz, while droop control showed oscillations up to 0.05 Hz.

### D. Voltage regulation

The proposed control framework reduces voltage deviations by 65% compared with droop control, as shown in Fig. 4. The adaptive  $m_Q$  coefficient adjusted reactive power sharing based on line impedance, minimizing  $\Delta V$  to  $\pm 4.8$  V. Fixed-inertia VSG lacked this adaptability, rather leading to  $\pm 8.4$  V deviations.

### E. Adaptive inertia and BESS performance

During DG loss,  $H(t)$  increased by 62.5% (from 4 to 6.5 s), enhancing the transient stability. By contrast, the fixed-inertia VSG could not adapt, resulting in larger frequency swings. As shown in the response of the BESS SoC in Fig. 5, the multi-objective optimization maintained the SoC within 20%–80%, avoiding harmful deep

**TABLE I.** Algorithm of the proposed system.

Steps	Activities
System initialization	Set base parameters: adaptive VSG: $H_{base}, k_f, k_{SoC}$ BESS: $SoC_{min}, SoC_{max}$ Communication: event-triggered thresholds ( $\varepsilon_f, \varepsilon_V$ )
	Primary control layer (local, real-time)
Step 1	Measure local frequency ( $f$ ), voltage ( $V$ ), and BESS SoC
Step 2	Adjust VSG inertia dynamically using Eqs. (3) and (17)
Step 3	Apply adaptive Q-V droop for voltage regulation based on line impedance using Eqs. (19) and (21)
Step 4	Manage and dispatch power setpoints to DERs while maintaining SoC limits
	Secondary control layer (distributed, 0.1–1 s)
Step 1	Collect delayed neighbor states ( $f_j, V_j$ ) via event-triggered communication
Step 2	Compensate delays using Padé approximants using Eq. (12)
Step 3	Compute global corrections via consensus protocol using Eqs. (13) and (14)
Step 4	Update reference values ( $f_{ref}, V_{ref}$ ) for primary control
	Tertiary control layer (centralized, 1–5 min)
Step 1	Monitor system states ( $f, V$ ) and external inputs (energy prices, forecasts)
Step 2	Optimize BESS dispatch and DER setpoints using Eqs. (22)
Step 3	Adjust weighting factors ( $\alpha, \beta, \gamma$ ) based on priorities
	Event handling
Disturbance detection	Trigger re-initialization of control layers for sudden load/generation changes
Communication	Transmit data only if $ \Delta f  > \varepsilon_f$ or $ \Delta V  > \varepsilon_V$

discharges. Three cases (with 30%, 50%, and 80% initial status of SoC) were conducted to ensure the validity of BESS performance that could be maintained within 20%–80%. The results are illustrated in Fig. 5.

During DG loss, SoC dropped from 50% to 28% but recovered to 45% within 4 s. In the PV ramp-down event, the SoC increased to 72% owing to excess PV curtailment but stabilized at 68%.

## F. Communication efficiency

The event-triggered mechanism reduces data packets by 50% compared with the time-triggered systems in Ref. 43. Delays of up to 500 ms were compensated using Padé approximants, with no instability observed.

## IV. DISCUSSION

### A. Transient response of adaptive VSG

The dynamic inertia adjustment of the proposed framework directly addresses the low-inertia challenge in renewable-dominated microgrids. By coupling  $H(t)$  with the real-time frequency deviation and BESS SoC, the system emulates synchronous generator behavior more effectively than static VSG models.<sup>20</sup> For instance, a 62.5% increase in  $H(t)$  during DG loss reduced the rate of change of frequency (RoCoF) by 40%, aligning with the findings of Ref. 10 on virtual inertia.

### B. Voltage-inertia coupling

Existing VSG implementations often prioritize frequency stability at the expense of voltage regulation.<sup>11</sup> The integration of the

adaptive Q-V droop with VSG dynamics resolves this by dynamically adjusting  $m_Q$  based on line impedance. This reduced the voltage deviation by 65% compared to the conventional droop control, demonstrating the necessity of coupled control layers.

### C. BESS optimization trade-offs

The multi-objective framework balances three competing goals: inertia support, which can maximize the inertia constant  $H(t)$  during transients; voltage regulation, which minimizes the voltage deviation; and BESS longevity, which constrains SoC within predefined limits.

While the SoC dipped to a lower limit during DG loss, the recovery algorithm prioritized recharge during PV curtailment, ensuring long-term battery health. This aligns with the emphasis of Ref. 31 on decentralized SoC balancing.

### D. Robustness to communication constraints

The delay-compensated consensus protocol outperformed existing methods, such as bi-limit homogeneity<sup>15</sup> using predictive feedback, enabling the mitigation of actuator saturation during delays. Event-triggered communication can also reduce network traffic without compromising stability.

These features ensure scalability for larger microgrids with heterogeneous communication networks.

### E. Limitations and practical challenges

The simulation assumed ideal line impedance matching. In real-world systems with asymmetric impedance, voltage deviations may increase slightly.

**TABLE II.** System parameters.

Parameter	Value	Remark
(1) Microgrid configuration		
$P_{rated}$	500 kW	System capacity
$V_{nom}$	400 V	Nominal voltage
$f_{nom}$	50 Hz	Nominal frequency
$Z_{line}$	$0.1 + 0.05j \Omega$	Line impedance
(2) Component parameters		
$P_{PV}$	250 kW	PV capacity
$P_{wind}$	100 kW	Wind capacity
$P_{DG}$	150 kW	Diesel generator capacity
$P_{load}$	500 kW	Load demand
$P_{BESS}$	100 kW	BESS capacity
$E_{BESS}$	100 kWh	BESS energy capacity
(3) Disturbance parameters		
$P_{loss}$	150 kW	Case 1: 150 kW DG loss at $t = 2$ s
$P_{PV-initial}$	$0.5 * P_{base}$	Case 2: PV generation (250 kW)
$P_{surge}$	$0.2 * P_{load}$	Case 2: 20% load surge at $t = 5$ s
(4) Control parameters		
(4.1) Adaptive VSG parameters		
$H_{base-adaptive}$	4	Base inertia (s)
$k_f$	0.8	Frequency gain (s/Hz)
$k_{SoC}$	0.2	SOC gain (s)
D	0.01	Damping coefficient (pu)
$m_Q$	$7.5 \times 10^{-4}$	Q-V droop coefficient (V/kVAR)
$k_z$	0.01	Q-V droop sensitivity (pu)
(4.2) Fixed VSG parameters		
$H_{base}$	4	Base inertia (s)
D <sub>fixed</sub>	0.01	Damping coefficient (pu)
$m_{Q-fixed}$	$7.5 \times 10^{-4}$	Q-V droop coefficient (V/kVAR)
(4.3) Droop parameters		
$m_p$	0.05	Frequency droop coefficient (Hz/kW)
$n_q$	$7.5 \times 10^{-4}$	Voltage droop coefficient (V/kVAR)
(4.4) BESS parameters (for adaptive VSG)		
$SoC_{initial}$	30%, 50%, 80%	Initial SOC
$SoC_{min}$	20%	Minimum SOC
$SoC_{max}$	80%	Maximum SOC
Charge efficiency	95%	
Consensus gain	0.5	Secondary layer gain
$\epsilon$	0.02 Hz/V	Event threshold
(5) Simulation parameters		
$t_{sim}$	10	Simulation time
$dt$	0.001	Time step
$t$	(0:dt:tsim)	Time vector

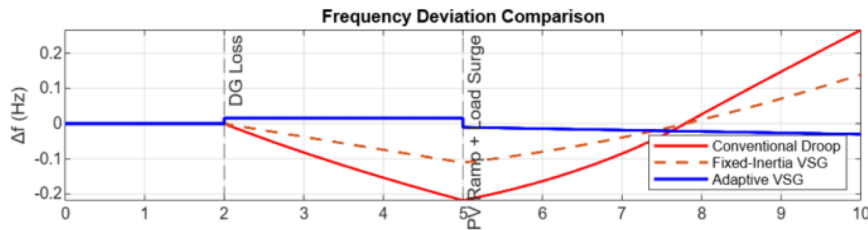


**FIG. 3.** Frequency response of the system comparing the proposed system with the selected benchmarks.

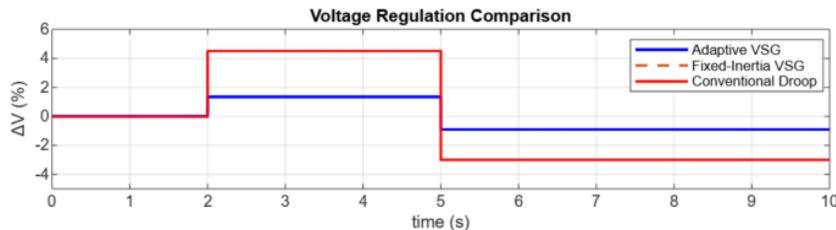
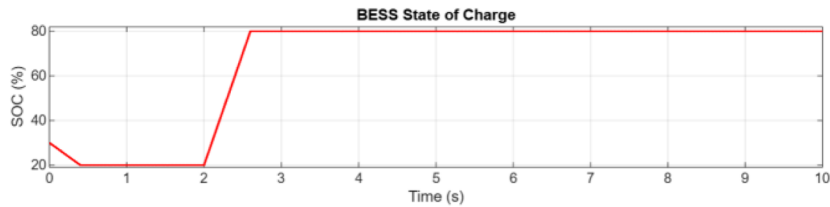
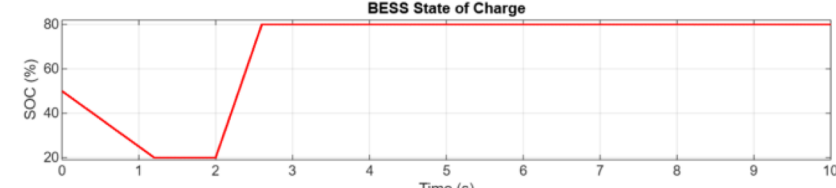


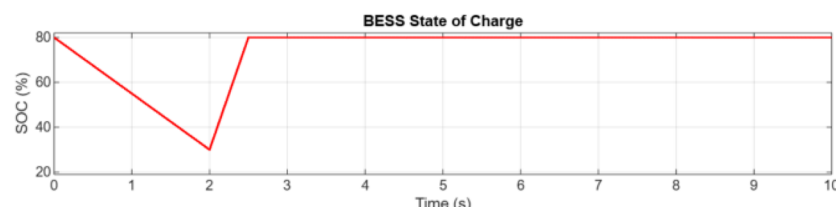
**FIG. 4.** Voltage response of the system comparing the proposed system with the selected benchmarks.



(a)



(b)



(c)

**FIG. 5.** BESS state of charge (SoC) response of the system comparing the proposed system with the selected benchmarks at the initial state of charge with (a) 30%, (b) 50%, and (c) 80%.

Another limitation is that while the framework is modular, integrating attack detection modules (e.g., BiLSTM networks from Ref. 42) is essential for field deployment.

However, hardware compatibility is a practical challenge. Adaptive VSG requires high-speed controllers for real-time inertia adjustment, which may increase implementation costs.

In general, the results validated the proposed hierarchical framework as a robust solution for frequency and voltage stability in low-inertia microgrids. By dynamically adjusting inertia,

compensating for communication delays, and optimizing BESS usage, the critical gaps in existing methods are addressed.

## V. CONCLUSIONS

This paper proposes a hierarchical control framework to address the key challenges of frequency and voltage instability in islanded microgrids with high renewable energy penetration. By integrating adaptive VSG dynamics, a delay compensation

consensus protocol, and optimized BESS management, the framework significantly improves the transient stability and operational resilience of the system. The main contributions of this study are as follows:

- The adaptive VSG dynamically adjusts the inertia constant according to the real-time frequency deviation and SoC of the BESS, which reduces the frequency minimum point by 60% compared with the fixed inertia VSG and 70% compared with the traditional droop control. This adjustment ensured the robustness of the system during load fluctuations and intermittent renewable energy periods.
- By embedding adaptive Q-V droop control in the VSG architecture, the voltage deviation is successfully minimized to  $\pm 1.2\%$ , overcoming the decoupled control limitation in the conventional approach.
- Combining a delay compensation consensus protocol and an event-triggered communication mechanism, the system is kept stable under a communication delay of 500 ms while reducing network traffic by 50%.
- A multi-objective optimization strategy is adopted to balance synthetic inertial support, voltage regulation, and SoC constraints while enhancing grid stability and maintaining battery health (SoC is controlled in the range of 20%–80%).

Simulation results verified that the framework performed well in a 500 kW microgrid with 70% renewable energy penetration, a stabilization time 30% faster than the baseline, and a 65% reduction in voltage deviation. However, this study assumes ideal line conditions and does not consider cyber-attack resilience, thus emphasizing future research directions.

Future studies should focus on hardware-in-the-loop validation, cost-effectiveness, and cyberattack resilience testing. If so, bridging the gap between theoretical innovation and practical application, this study paves the way for resilient, renewable energy-dominated microgrids in the era of energy transition.

## ACKNOWLEDGMENTS

We acknowledge the Bahir Dar Institute of Technology, Bahir Dar University, for supporting this work with the materials and experiments.

## AUTHOR DECLARATIONS

### Conflict of Interest

The authors have no conflicts to disclose.

### Author Contributions

**Girmaw Teshager Bitew:** Conceptualization (equal); Data curation (equal); Formal analysis (equal); Methodology (equal); Software (equal); Validation (equal); Writing – original draft (equal); Writing – review & editing (equal). **Teketay Mulu Beza:** Project administration (equal); Resources (equal); Supervision (equal). **Muhammad Shahzad:** Validation (equal); Visualization (equal).

## DATA AVAILABILITY

MATLAB code is available for this manuscript.

## ABBREVIATIONS

BESS	battery energy storage system
BiLSTM	bidirectional long short-term memory
DoS	denial-of-service
MPC	model predictive control
SoC	state of charge of BESS
VSG	virtual synchronous generator

## APPENDIX: SYSTEM PARAMETERS

Table II shows the system parameters.

## REFERENCES

- S. Nema, V. Prakash, and H. Pandzic, “Adaptive synthetic inertia control framework for distributed energy resources in low-inertia microgrid,” *IEEE Access* **10**, 54969–54979 (2022).
- J. Pahasa, P. Potejana, and I. Ngamroo, “MPC-based virtual energy storage system using PV and air conditioner to emulate virtual inertia and frequency regulation of the low-inertia microgrid,” *IEEE Access* **10**, 133708–133719 (2022).
- W. M. Hamanah, Md. Shafiullah, L. M. Alhems, M. S. Alam, and M. A. Abido, “Realization of robust frequency stability in low-inertia islanded microgrids with optimized virtual inertia control,” *IEEE Access* **12**, 58208–58221 (2024).
- C. Li, Y. Yang, T. Dragicevic, and F. Blaabjerg, “A new perspective for relating virtual inertia with wideband oscillation of voltage in low-inertia DC microgrid,” *IEEE Trans. Ind. Electron.* **69**(7), 7029–7039 (2022).
- I. Todorovic, I. Isakov, D. Reljic, D. G. Jerkan, and D. Dujic, “Mitigation of voltage and frequency excursions in low-inertia microgrids,” *IEEE Access* **11**, 9351–9367 (2023).
- M. Samadi and J. Fattahi, “Low-inertia microgrid synchronization using data-driven digital twins,” *IEEE Access* **12**, 78534–78548 (2024).
- I. Ngamroo and T. Surinakaew, “Control of distributed converter-based resources in a zero-inertia microgrid using robust deep learning neural network,” *IEEE Trans. Smart Grid* **15**(1), 49–66 (2024).
- B. Yildirim, M. Gheisarnejad, and M. H. Khooban, “A new parameter tuning technique for noninteger controllers in low-inertia modern power grids,” *IEEE J. Emerg. Sel. Top. Ind. Electron.* **3**(2), 279–288 (2022).
- D. Zheng *et al.*, “Key technical challenges in protection and control of microgrid,” in *Microgrid Protection and Control* (Elsevier, 2021), pp. 45–56.
- M. Chethan and K. Ravi, “Virtual inertia support for renewable energy integration: A review,” *IEEE Access* **13**, 11517–11531 (2025).
- Y. Li, J. Liu, J. Liu, and J. Xu, “Simultaneous voltage and current harmonic control of grid-forming converters considering both islanded and grid-connected modes,” *IEEE Trans. Ind. Electron.* **72**(2), 1649–1660 (2025).
- A. Afshari, M. Raeispor, M. Davari, W. Gao, F. Blaabjerg, and T. Chai, “Finite-rate distributed secondary control over digital communication networks using an event-triggered quantized algorithm for islanded modern microgrids utilizing inverter-based resources,” *IEEE Trans. Ind. Inf.* **21**(2), 1002–1016 (2025).
- R. Musona and I. Serban, “Control of a single-phase islanded microgrid based on virtual oscillator control enhanced with power limitation and robust distributed secondary control,” *IEEE Open J. Ind. Electron. Soc.* **6**, 25–42 (2025).
- W. Zhang, G. Teshaer Bitew, D. Zheng, S. Netsanet alemu, D. Wei, and X. Zhang, “An improved dynamic control and resonance damping for voltage source inverters in microgrids through a novel active damping technique,” *Am. J. Electr. Power Energy Syst.* **11**(1), 11 (2022).
- Q. Wang *et al.*, “Distributed secondary control based on Bi-limit homogeneity for AC microgrids subjected to non-uniform delays and actuator saturations,” *IEEE Trans. Power Syst.* **40**(1), 820–833 (2025).

- <sup>16</sup>X. Cai, B. Gao, X. Nan, and J. Yuan, "Resilient discrete-time quantization communication for distributed secondary control of AC microgrids under DoS attacks," *IEEE Syst. J.* **18**(3), 1798–1808 (2024).
- <sup>17</sup>J. Zhang, S. Fan, C. Deng, B. Wang, and X. Xie, "Distributed resilient secondary control for AC microgrids against hybrid attacks," *IEEE Trans. Circuits Syst. I* **71**(11), 5211–5220 (2024).
- <sup>18</sup>D. Zheng *et al.*, "Tertiary control of microgrid," in *Microgrid Protection and Control* (Elsevier, 2021), pp. 255–295.
- <sup>19</sup>Q. Wu, X. Chu, Y. Fan, L. Liu, and X. Sun, "Consistency algorithm-based SOC balancing scheme of retired non-equal capacity lithium battery in virtual synchronous generator controlled microgrids," *IEEE Access* **13**, 9073–9088 (2025).
- <sup>20</sup>J. Ou, H. Han, G. Shi, Y. Guan, A. Lashab, and J. M. Guerrero, "An improved  $\omega\phi$  droop control for cascaded PV-ES system in islanded mode," *IEEE Trans. Sustainable Energy* **16**(1), 45–61 (2025).
- <sup>21</sup>I. Alotaibi and M. Abido, "Robust  $H_{\infty}$  based virtual synchronous generators for low inertial microgrids considering high penetration of renewable energy," *IEEE Trans. Ind. Appl.* **60**(6), 8341–8352 (2024).
- <sup>22</sup>C. Liu, Z. Chu, Z. Duan, and Y. Zhang, "VSG-based adaptive optimal frequency regulation for AC microgrids with nonlinear dynamics," *IEEE Trans. Autom. Sci. Eng.* **22**, 1471–1482 (2025).
- <sup>23</sup>Z. Zeng *et al.*, "A model predictive control with grid-forming capability for back-to-back converters in wind turbine systems," *IEEE Open J. Power Electron.* **5**, 1697–1708 (2024).
- <sup>24</sup>K. Ma *et al.*, "Distributed resilient control for frequency/voltage recovery and power sharing in seaport microgrids with all-electric ships," *IEEE Trans. Transp. Electrif.* **11**(1), 4070–4082 (2025).
- <sup>25</sup>A. Matthee, N. Moonen, I. Sulaeman, and F. Leferink, "Transient response of generator- and inverter-based microgrids to rapid load changes," *IEEE Trans. Electromagn. Compat.* **66**(5), 1646–1654 (2024).
- <sup>26</sup>S. Bhattacharyya and B. Singh, "Operation of a standalone microgrid with an advanced discrete generalized integrator based FLL control," *IEEE Trans. Power Deliv.* **39**(6), 3233–3242 (2024).
- <sup>27</sup>S. Chakraborty, G. Modi, B. Singh, and B. K. Panigrahi, "A variable linear coefficient battery cost function embedded control for revenue maximization of grid tied solar photovoltaic system," *IEEE Trans. Ind. Appl.* **61**(1), 1220–1233 (2025).
- <sup>28</sup>Q. Tang, C. Deng, S. Fan, Y. Wang, D. Yue, and B. Wang, "A novel cooperative resilient control method for energy storage systems under hybrid attacks," *IEEE Trans. Ind. Electron.* **72**(2), 1871–1880 (2025).
- <sup>29</sup>S. E. Sati, A. Al-Durra, H. Zeineldin, T. H. M. El-Fouly, and E. F. El-Saadany, "A novel virtual inertia-based damping stabilizer for frequency control enhancement for islanded microgrid," *Int. J. Electr. Power Energy Syst.* **155**, 109580 (2024).
- <sup>30</sup>L. Toma *et al.*, "On the virtual inertia provision by BESS in low inertia power systems," in *2018 IEEE International Energy Conference (ENERGYCON)* (IEEE, Limassol, 2018), pp. 1–6.
- <sup>31</sup>T. A. Fagundes *et al.*, "Battery energy storage systems in microgrids: A review of SoC balancing and perspectives," *IEEE Open J. Ind. Electron. Soc.* **5**, 961–992 (2024).
- <sup>32</sup>M. A. Ebrahim, A. M. El-Rifaie, B. A. Bahr, H. E. Keshta, M. N. Ali, and M. M. R. Ahmed, "Adaptive control of a hybrid microgrid with energy storage system," *IEEE Open J. Power Electron.* **6**, 196–211 (2025).
- <sup>33</sup>J. Zhang, S. M. Mohiuddin, and J. Qi, "Virtual agents-based attack-resilient distributed control for islanded AC microgrid," *IEEE Access* **13**, 15825–15839 (2025).
- <sup>34</sup>H. Baocheng, C. Yueliang, L. Quan, H. Zhengdong, G. Yuan, and Y. Hairui, "Frequency and voltage regulation strategy of microgrid based on energy storage virtual synchronous generator technology," in *2021 IEEE 2nd International Conference on Information Technology, Big Data and Artificial Intelligence (ICIBA)* (IEEE, Chongqing, China, 2021), pp. 17–21.
- <sup>35</sup>O. Obreh-Snapps, R. Bo, B. She, F. F. Li, and H. Cui, "Improving virtual synchronous generator control in microgrids using fuzzy logic control," in *2022 IEEE/IAS Industrial and Commercial Power System Asia (I&CPS Asia)* (IEEE, Shanghai, China, 2022), pp. 433–438.
- <sup>36</sup>A. Kumar and M. De, "Effectiveness of Zeigler-Nicholas method based parameter tuning of virtual synchronous generator for LFC in low inertia islanded microgrid," in *2022 IEEE Delhi Section Conference (DELCON)* (IEEE, New Delhi, India, 2022), pp. 1–6.
- <sup>37</sup>K. C. Bandla, M. V. Gururaj, and N. P. Padhy, "Decentralized and coordinated virtual synchronous generator control for hybrid AC-DC microgrids," in *2020 IEEE International Conference on Power Electronics, Smart Grid and Renewable Energy (PESGRE2020)* (IEEE, Cochin, India, 2020), pp. 1–6.
- <sup>38</sup>H. Li, "Research on power decoupling method of virtual synchronous generator in islanded microgrid," in *2019 6th International Conference on Dependable Systems and Their Applications (DSA)* (IEEE, Harbin, China, 2020), pp. 526–528.
- <sup>39</sup>L. Ning, Z. Xiang, C. Yujie, H. Fuxing, Z. Shiqian, and W. Yelin, "Virtual synchronous generator technology and its parallel control strategy in isolated island microgrid," in *2019 IEEE 10th International Symposium on Power Electronics for Distributed Generation Systems (PEDG)* (IEEE, Xi'an, 2019), pp. 316–320.
- <sup>40</sup>A. Ito, A. Kawashima, T. Suzuki, S. Inagaki, T. Yamaguchi, and Z. Zhou, "Model predictive charging control of in-vehicle batteries for home energy management based on vehicle state prediction," *IEEE Trans. Contr. Syst. Technol.* **26**(1), 51–64 (2018).
- <sup>41</sup>S. Tyagi, B. Singh, and S. Das, "Control of interlinking converter for power quality improvement in hybrid microgrid," *IEEE Trans. Ind. Electron.* **72**(2), 1607–1616 (2025).
- <sup>42</sup>M. Z. Shahabadi, H. Atrianfar, G. B. Gharehpetian, and A. Yazdani, "Distributed self-triggered control of islanded microgrids under switching communication topologies," *IEEE Trans. Ind. Inf.* **20**(12), 13904–13915 (2024).
- <sup>43</sup>K. Zhao, F. Xiao, S. Li, X. Wang, and B. Wei, "Distributed secondary control of microgrids via a time-event switching triggered mechanism," *IEEE Control Syst. Lett.* **8**, 2463–2468 (2024).